Research Article

Synthesis, Characterization and Antimicrobial Properties of Manganese Doped Zinc Sulphide Nanoparticles

JanmejayYadav[1] , **Vikram Singh**[2] , **Ram Kripal**[3*] , **Rajesh Kumar Yadav**[4] , **Urvashi Srivatava**[5]

[1,2]Dept. of Physics, Nehru Gram Bharati (Deemed to be University), Jamunipur, Prayagraj, India
[3]EPR Laboratory, Department of Physics, University of Allahabad, Prayagraj, India
[4]Dept. of Physics, CMP Degree College, University of Allahabad, Prayagraj, India
[5]Dept. of Home Science, Prof. Rajendra Singh (Rajju Bhaiya) University Prayagraj, India

Corresponding Author: ✉

Abstract— This paper focuses on the controlled size of manganese-doped zinc sulfide nanocrystalline powders made via an easy-to-understand aqueous chemical procedure that eliminates the requirement for a capping agent. It was examined by the size of the ZnS nanoparticles was exaggerated by varying calcination temperatures. Rendering to W-H analysis, ZnS nanoparticles' average crystallite size rose as the calcination temperature rose Spectroscopy of UV-vis in diffused reflectance (DR) mode was employed to analyze optical properties, It demonstrated a notable reflective feature at 420 nm at 500 ∘C calcination temperature and a sharp rise in reflectivity at 375 nm. Morphology and elemental compositions were investigated via transmission electron microscopy (TEM) and scanning electron microscopy (SEM). As the calcination temperature was elevated, ZnS nanoparticles' average crystallite size grew in accordance with Scherrer's formula and W-H analysis. UV–vis spectroscopy in diffused reflectance (DR) mode was employed to analyze optical properties, which, at 500 ∘C calcination temperature, had a notable reflective characteristic after 420 nm and a sharp rise in reflectivity at 375 nm. In comparison with pure ZnS NPs, Mn-doped ZnS (15 mol%) NPs shown greater antibacterial activity against *Shigellaflexneri, Salmonella typhi, E. coli,* and *Staphylococusaureus*.

Keywords— Mn-doped nanoparticles, zinc sulfide, Scherrer's equation, Transmission electron microscopy, Antibacterial activity, nanoparticles

1. Introduction

More than 25 years have passed since the discovery of nanocrystalline materials [1]**.** Their peculiar characteristics, which derive from the high atom concentration at the interfacial structure and the comparatively easy methods of production, are the primary cause. Because of its potential uses in molecular electronics, nonlinear optics, sensors, catalysis, and other fields, zinc sulfide nanoparticles have recently been the focus of extensive research [2, 3]**.** Simultaneously, more research is required to synthesize zinc sulfide (ZnS) particles with a limited size variation and consistent shape. Numerous chemical methods for preparing nanoparticles have been developed as a result of the growing interest in these materials. These methods include sputtering [4], co-evaporation [5], ultrasound irradiation [6], Microwave irradiation [12], ion complex transformation [11], gas-phase condensation [9], liquid-phase chemical precipitation [10], solid-state reaction [8], sol–gel technique [7], and biological transformation [13]. From all of these studies, it has been determined that the particular preparation technique used as well as the applied experimental circumstances significantly affect the size of the particlesand luminous characteristics of ZnS powders. This work is the first in a series devoted to comparing the morphostructure of ZnS:Mn particles in nanocrystalline form using various synthesis techniques. In this regard, precipitation is the method used in attempts to produce manganese doped ZnS nanoparticles. ZnS: Mn nanoparticles were analyzed using techniques such as transmission electron microscopy (TEM) and scanning electron microscopy (SEM). This part addressed the study's goal and provided an overview of the study. The paper's remaining sections are arranged as follows. The pertinent work from previous researchers on the production and evaluation of zinc sulfide nanoparticles doped with manganese is included in Section 2.

Section 3 describes the methods for figuring out how to make manganese-doped zinc sulfide nanocrystalline powder. Section 4 outlines the process. The results and discussion are shown in Section 5. Section 6 discusses the study's findings and future directions.

2. Related Work

Maskaeva et al. [14] used chemical deposition on frosted glass substrates. They created CuS(Mn) and CuS(Ni) powders and thin films doped with nickel or manganese. The thickness of these materials varied between 170 and 200 nm. It was shown that CuS-based dispersions displayed the hexagonal crystalline structure by the use of X-ray diffraction. Venkatarao et al. [15] studied the ZnS-MoS$_2$. Semiconducting natured undoped and Mn^{2+} doped nanocomposites were prepared by bottom-up hydrothermal synthesis. Using X-ray diffraction analysis (XRD), diffuse reflection spectroscopy (DRS), Fourier transform infrared spectroscopy (FT-IR), scanning electron microscopy (SEM), and PL photoluminescence techniques, the structural, optical absorption, morphological, infrared spectral, and luminescence properties of the produced powder samples were assessed. They reported the produced nanocomposites of an average crystallite size of 12–20 nm. The produced samples' different functional groups and molecular vibrations were investigated using the FT-IR spectra. Mostafa et al. [16] focused on characterizing Mn-doped ZnS. They employed a straightforward wet chemical technique to create highly photoluminescent (PL) material, which they then covered with 3-mercaptopropionic acid (MPA). They created ZnS doped with Mn. X-ray diffraction (XRD), High resolution transmission electron microscopy (HRTEM), and fluorescence emission spectra were used to evaluate the generated Mn doped ZnS QDs (quantum dots) and the pure ZnS QDs.

Mn-doped ZnS QDs had dual emission peaks at 425 and 570 nm, whereas pure ZnS QDs exhibited a very weak emission PL Gaussian peak at about 395 nm. Mn^{2+} doped and Cu^{2+}-included Sn$_2$S$_3$ nanocrystals (NCs) created by chemical bath deposition were reported by Noppakuadrittidej et al. [17]. The Cu^{2+} ions formed an anorthic Mn^{2+}-doped Cu$_2$SnS$_3$ structure with E$_g$ = 1.44 eV, which altered the material's optical and photo/electrochemical properties. Photoluminescence spectra blue shifted from 411.69 nm to 411.13 nm after Mn^{2+}-doped Sn$_2$S$_3$ or Mn^{2+}-doped Cu$_2$SnS$_3$ NCs were applied to the bare Nb$_2$O$_5$ electrode.

The Cu^{2+}-incorporated sample showed a slightly higher emission at the same place as the sample without Cu^{2+}, according to changes at the interface of Mn^{2+}-doped Cu$_2$SnS$_3$ NCs. The crystalline structure's disarray might be the reason of this. They claimed that since the Mn^{2+}-doped Cu$_2$SnS$_3$ had a greater electroactive surface area, electrochemical testing demonstrated a decreased charge transfer resistance. Bansal and associates [18] developed the undoped and transition metal (Cu, Mn, and Cu: Mn) doped ZnS nanoparticles by using an aqueous synthesis method. They studied structural and optical properties of synthetic materials by using a variety of techniques. They reported the crystallite sizes of undoped, Cu, Mn, and Cu: Mn doped ZnS nanoparticles as 1.68, 1.87, 1.50, and 1.42 nm, respectively, based on X-Ray diffraction (XRD). XRD, Selected Area Electron Diffraction, and High Resolution Transmission Electron Microscopy all confirm that ZnS nanoparticles have a stable hexagonal phase at low temperatures.

Energy dispersive spectroscopy was used to verify nanoparticle doping. The blue shift in UV absorbance shows that the optical band gap rises as particle size falls.

Using the chemical precipitation approach, Rao et al. [19] created the ZnO-CdS composite nanopowder doped with Mn2+. Their optical, magnetic, and structural characteristics were examined in relation to Mn^{2+} doping. This investigation indicates that the average crystallite size is 18 nm, and the XRD pattern shows the hexagonal phase of both ZnO and CdS. The morphological investigations reveal irregularly dispersed, spherically shaped structures with minimal aggregation.

The special electrical and semiconducting characteristics of metal sulfide nanoparticles were the main focus of Athanassio et al. [20]. By cautiously altering the sulfur amount and composition of the flame gas, the formation of oxide nanoparticles in flames may be expanded to sulfides.

Ni-doped ZnS NPs were created by Munir et al. [21], who also investigated their characterisation by in-vitro bioassays employing the well diffusion method to evaluate their antiseptic and anticancer qualities against *B. cereus, E. coli,* and the HepG2 liver cancer cell line. The data provide impressive results, with a maximum inhibition zone of around 9 to 23 mm against *E. coli* and 12 to 27 mm against *B. cereus*, respectively. Saroja et al. [22] used the in vitro disk diffusion technique, for the antibacterial activity of the ZnS thin film as deposited against a variety of pathogens. According to them from this experiment Mn doped ZnS thin film revealed better antibacterial activity and photo catalytic degradation capabilities in comparison to undoped ZnS thin film.

Ali, et al. [23] used a co-precipitation technique to produce the cubic zinc blende structure's manganese-doped zinc sulfide nanoparticles, which had an average crystallite size of around 3.56 nm.

By utilizing the well diffusion technique to measure the width of the inhibition zone against two different bacterial strains, the antibacterial activity of (ZnS: Mn^{2+}) nanocrystals was examined. The inactivation method of microorganisms was thought to be sort-dependent. Bacillus subtilis showed the highest antibacterial sensitivity (35 mm) to ZnS: Mn2+ nanoparticles at a dosage of 50 mM, but *Escherichia coli* produced the largest zone of inhibition (20 mm) at the same concentration. The study's inferences showed that in clinical settings, ZnS: Mn2+ nanoparticles workwise repressed both Gram-positive (*Bacillus subtilis*) and Gram-negative (*E. coli*) bacteria.

3. Theory/Calculation

3.1 Scherrer's equation

The widening of a powder's powder diffraction peaks is related to its mean crystallite size by the Scherrer equation to get the crystallite size of that powder. By using Scherrer's equation to the X-ray line broadening approach, the crystallite size of the ZnS nanoparticles was determined:

$$D = \frac{K\lambda}{\beta_{hkl} \cos\theta} \frac{\kappa\lambda}{\beta hkl Cos\theta} \tag{1}$$

where λ is the wavelength of the Cu K_α radiation (1.5406 ˚A),), K is the form factor (0.9), β_{hkl} is the scattering angle, D is the crystallite's size, and FWHM is the full width at half maximum (FWHM) in radians [24].

3.2 Williamson–Hall analysis

Average coherently diffracting domain size and strain can be determined using Williamson-Hall X-ray line broadening analysis. Because of crystal imperfections, strain-induced peak broadening occurs; and distortion, which had been computed utilizing the relationship:

$$\varepsilon = \frac{\beta_{hkl}}{4\tan\theta} \tag{2}$$

A modified Scherrer's formula was proposed by Williamson and Hall and was computed using the relation [25]:

$$\beta_{hkl}\cos\theta = \frac{K\lambda}{D} + 4\varepsilon\sin\theta \tag{3}$$

3.3 Optical study: UV-vis analysis

A theoretical method for examining how a substrate's color changes following the application of a paint layer is the K-M model. Kubelka-Munk function was used to calculate the band gap energies [26].

$$F(R) = \frac{(1-R)^2}{2R} \tag{4}$$

In this case, the absorption coefficient is equal to F(R), and (R) is the reflectance's absolute value. An estimate of ZnS's direct band gap was obtained by graphing

$$[F(R)\cdot h\nu]^2 \text{ vs. } h\nu \text{ (eV)} \tag{5}$$

4. Experimental Method

This section has been divided into two parts, first part describes the experiment procedure of manganese doped zinc sulphide nano crystalline powder and second part of the section describes the characterization of nanoparticles.

4.1 Synthesis of ZnS nanoparticles

All of the chemical reagents used in the experiment, namely Merck with 99% purity, were analytical grade and required no further purification for the formation of ZnS nanoparticles. This study aimed to produce controlled-dimension manganese-doped zinc sulphide ZnS: Mn^{2+} nanoparticles. Zn-Mn acetate combination and sodium sulfide were the starting points for the preparation of ZnS: Mn^{2+} powders, with the addition of methacrylic acid as a particle size regulator. The SeqAdd approach was utilized to produce precipitation at a low temperature. ZnS nanoparticles with varying Mn-doping levels were produced by using Zn-Mn acetate solutions of different compositions. Zn-Mn double sulphide is the precipitation product that was formed, and the general equation for the chemical reaction can be used to explain it:

$$(1-x)Zn(CH_3COO)_2 + xMn(CH_3COO)_2 + Na_2S \longrightarrow$$
$$(1-x)ZnS.xMnS + 2CH_3COONa$$
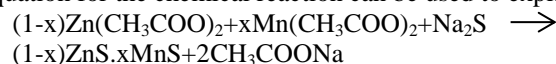
The sample was made in this way using a combination that included the Mn/(Zn+Mn) ratios: 15 mol%. It must be mentioned that the quantity of included Mn is around 0.1%.
Mn-doped ZnS powders were made by precipitating Zn-Mn acetate and sodium sulfide in an aqueous solution at low temperatures (5°C) using the SeqAdd technique. This was proficient by producing a Zn-Mn acetate amalgamation with 15 mol Mn/100 mol (Zn+Mn) from 1M $Zn(CH_3COO)_2$ and 1M $Mn(CH_3COO)_2$ solutions, which was then diluted with deionized water that included α-methacrylic acid (MA). After adding the Na_2S aqueous explanation drop by drop to the mixed solution above, it was rapidly tense for half an hour. Following centrifugation and washing, the resultant powder was vacuum-dried at 80°C. The washing procedure was carried out using isopropyl alcohol and deionized water. In contrast, pure ZnS nanoparticles were also made with the aforementioned technique.

4.2 Characterizations

The Rigaku X Ray Diffractometer (Model: Smart Lab) was used to collect ZnS nanoparticle powder X-ray diffraction data. 3 KW. Micro Universal Testing Machine (Micro UTM) for Scanning Electron Microscopy (SEM) Tensile Stage Module Model: EVO MA 5 Micro Test 5000W: The elemental compositions and morphology were examined using a 5000N load cell. The size and form of the particles were shown in studies using scanning electron microscopy (SEM) and transmission electron microscopy (TEM).

The antibacterial efficacy of ZnS and Mn^{2+} doped ZnS NPs against gram negative *Salmonella typhi, Shigellaflexneri,* and *E. coli* bacteria as well as gram positive *Staphylococcus aureus*bacteria was assessed using the disc diffusion technique. They report the related activity indexes.

5. Results and Discussion

5.1 X-ray diffraction analysis of ZnS nanoparticles

Figure 1(a, b) illustrates the impact of various calcination temperatures on pure ZnS and Mn doped ZnS (15 mol%) nanoparticles. The fact that all of the peaks sharpened at

temperatures above 200 °C supports the idea that crystals can develop at higher calcination temperatures. Figure 1 makes it evident that ZnS only produced one phase, which is the hexagonal phase. When compared to lower calcination temperatures, Higher-temperature-calcined ZnS nanoparticles travel at peak places.

(1 11), (220), and (311) towards the lower Bragg's angle. Table 1 displays the average crystallite size of the ZnS nanoparticles, which was determined by calculations to be between 28 and 42 nm.
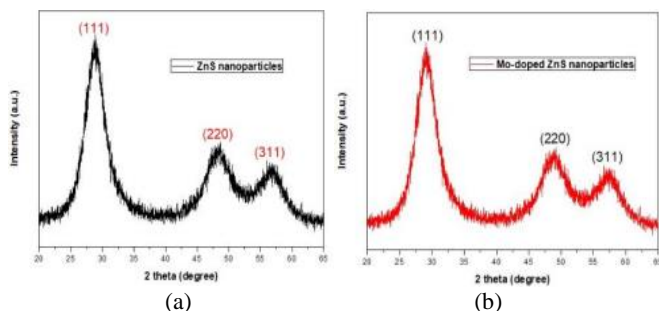

Fig. 1. Powder X-ray diffraction patterns of ZnS nanoparticles (a) The recorded XRD patterns for ZnS nanoparticles (b) The recorded XRD patterns for Mn-doped ZnS nanoparticles(15mol%)

One of the most used quantitative analytic tools for estimating crystallite size is still the X-ray diffraction (XRD). Although the Scherrer formula is often employed to predict nanostructural parameters, it overlooks the significant intrinsic strain contribution and only takes into account the impact of crystallite size on the XRD peak broadening [27, 28]. The size of articulately deflecting fields and the spreading of lattice coefficients from lattice disarticulations are dignified by lattice strain and crystallite size, respectively [29]. The point blemish, scrap frontier, and amassing culpabilities are the main grounds of the lattice strain subsequently to doping, which may eventually cause lattice extension or reduction in the nanocrystals [30]. As the attentiveness of Mn^{2+} ions increases, the preoccupation peaks shift to the longer wavelength side [31].

The flared in Bragg's peaks is presumed by the abridged WH indicative tool to be the total of peak lengthening brought on by persuaded strain and partial crystallite size [30, 32]. Since the crystallite size of as-synthesised ZnO (as determined by XRD) is knowingly greater than the Bohr stirring radius of ZnO, which is 2.34 nm, the increase in band gap or blue shift in absorption may not be the result of the quantum confinement effect. [33]. Rather, the Burstein-Moss effect, which has been well documented in the literature (for ZnO), has been credited causing a comparable band gap widening [34, 35].

Table1. Comparison of the geometric parameters of Mn-doped ZnS (15 mol%) nanoparticles obtained from Scherrer's formula and W–H analysis at 150°C, 300°C and 500°C

Calcination temperature (°C)	Average crystallite size, D (nm)		
	Scherrer's D (nm)	Williamson–Hall analysis	
		D (nm)	E
150	28	47	0.0076
300	39	66	0.0054
500	42	70	0.0038

The linear plot of $\beta_{hkl}\cos\theta$ against $4\sin\theta$ for the Mn-doped ZnS (15mol %) calcined at 150 °C, 300 °C, and 500 °C temperatures shown in Figure. 2 is represented by Eq. (3). The plots' slope yields the strain (ε) values, which are 0.0071, 0.0045, and 0.0056, in that order. Using the XRD-derived crystallite sizes (Scherrer's formula), where tiny ε lead to large crystallite size, the results made sense. Small grain size and small crystallite size were caused by large ε. The results of the calculations demonstrated that the strain linked to the samples reduced as the crystallite size progressively grew as the calcination temperature rose from 150 °C to 500 °C, as indicated in Table1.
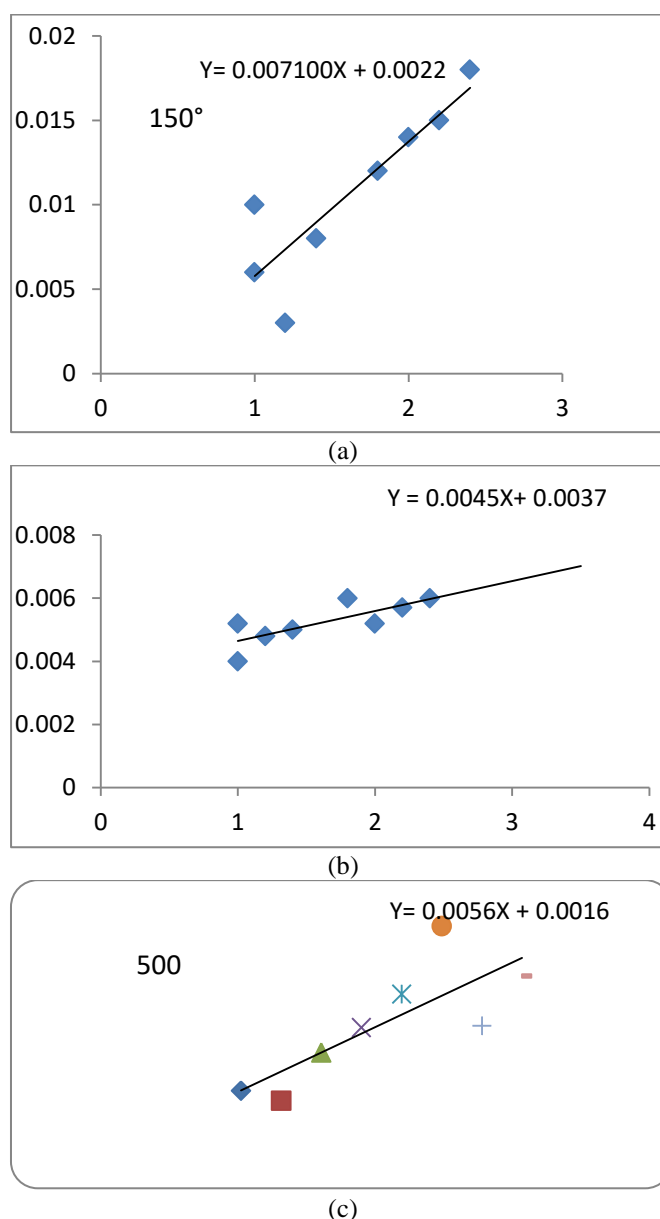

(a)

(b)

(c)

Fig. 2. Williamson–Hall analyses of ZnS nanoparticles calcined at (a) 150◦C, (b) 300 ◦C and (c) 500 ◦C temperatures assuming UDM plot.

5.2 Morphological evaluation

Investigations using scanning (SEM) and transmission (TEM) electron microscopy provided proof of the morphology and particle size. ZnS: Mn^{2+} powder, according to the SEM picture of the 15 mol% sample, is composed of 1-3 μm aggregates of closely spaced particles that are less than 45 nm (Fig. 3). The same sample's TEM image (Fig. 4) demonstrates that, in reality, the ZnS: Mn^{2+} powder is made up of minuscule particles, or quantum dots, that have dimensions smaller than three nanometers. These nanoparticles exhibit a significant tendency to agglomerate into considerably bigger particles due to their high surface area. The Mn-doped ZnS (15 mol %) ' crystallite sizes were determined to be in the nanometer range based on the SEM pictures. The crystallite sizes grew from 28 nm to 44 nm when the calcination temperature amplified from 150 °C to 500 °C. The nucleation rate of the particles increased through the calcination temperature. This is because the crystal core-forming process was accelerated within a certain time frame by the enhanced super saturation of the reaction products. Under these conditions, the formation of the crystal nucleus becomes the governing phase of the reaction instead of grain development. As the temperature rises, it becomes evident that the rapid creation of crystal nuclei is causing a phenomenon known as "nuclear-aggregation," which causes the crystal nuclei to aggregate. One important factor influencing the final products' shape and structure (crystallineness) is the rate of particle aggregation. The greater variations in height (Z range) at the margins of larger grain samples were found to be intrinsically rougher than those of smaller grains. But in every instance, the morphologies were quite similar. One can infer a comparable conclusion from the SEM observation. It was discovered that the process parameters had a significant impact on the morphology.
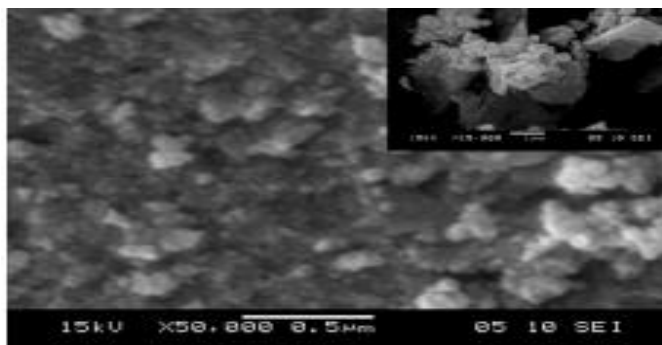

Fig. 3. SEM image of ZnS: Mn^{2+}(15 mol%)
(scale bar = 1 μm)

Fig. 4. TEM image of ZnS: Mn^{2+}(15 mol%,
(scale bar=50 nm)

The geometric properties of ZnS nanoparticles, as determined by W-H analysis and Scherrer's formula, are compiled in Table 1. By relating the regular crystallite size values resulting from W–H analysis, it was exposed that strain has a very trivial impression on the typical crystallite size of ZnS nanoparticles. The inconsistency in be an average of particle size dispersal was the purpose of the little difference in the regular crystallite size determined by Scherrer's formula and W-H analysis.

5.3 Optical study: UV-vis analysis

The findings of a study on the effects of varying calcination infections on the optical possessions of ZnS nanoparticles are exposed in Figure 5. The subtle reflectance spectra of the 500°C-calcined probationary exhibited a notable upsurge about 375 nm, and the substantial showed a high imitating feature beyond roughly 420 nm.

This resulted from the increased likelihood of photons with insufficient energy to engage with atoms or electrons reflecting back. It was shown that the particle sizes had a significant impact on the ZnS nanoparticles' ability to absorb. As the temperature rise from 150 °C to 500 °C, the obtained band gap energy (E_g) values were 3.13, 3.12, and 3.10 eV, respectively. The optical absorption edge somewhat migrated toward a longer wavelength in comparison to the reported band gap energy of bulk ZnS (E_g = 3.27 eV) [36]**.** Higher calcination temperatures may have increased grain size, which is what produced this change. [37]**.**
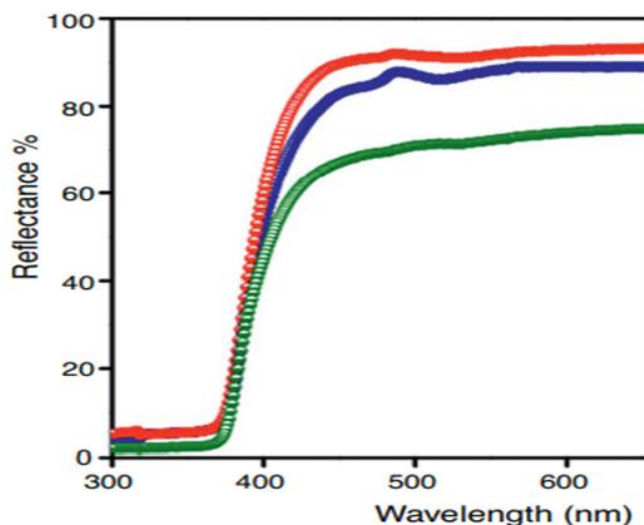

Fig 5. Diffuse reflectance spectra of the ZnO nanoparticles
calcined at 150°C, 300 ◦C and 500 ◦C temperatures

5.4 Antibacterial Activity

The antibacterial activity of ZnS and Mn2+doped ZnS NPs against gram positive ***Staphylococcus aureus*** and gram negative ***Shigella flexneri, E. coli bacterium, and Salmonella typhi*** was assessed using the disc diffusion technique.

They report the related action indexes. Figures 6 and 7 display the activity index for each catalyst as well as the zones of inhibition's average and standard deviation

After a 24-hour incubation period, Mn-doped ZnS shows strong bactericidal activity measured in terms of zone of inhibition (mm). Table 2 demonstrates that Mn-doped ZnS has better antibacterial efficacy against microorganisms than pure ZnS.

It is found that the Mn-doped ZnS standard error (SEM) and mean concentration needed for halting the development of *Staphylococusaureus Salmonella typhi, Shigellaflexneri and E. coli* are 18.08±2.02, 12.08±0.04, 16.3±1.12 and 13.8±0.10, respectively as accessible in Table 3. The increased activity of Mn-doped ZnS is caused by the improved adherence of Mn atoms to the cell walls of bacteria.It is generally accepted that metal ions bind to cell membranes via interfering with protein thiol groups, which inactivates respiratory enzymes. Moreover, it has been recommended that the improved electrostatic exchanges amid the NPs and the cell surface progressively modify the shape of the cell, cumulative penetrability and causing NPs to accumulate in the cytoplasm of the cell [38]. By encouraging lipid peroxidation and inner oxidative stress, the accumulating NPs damage DNA **[**39]**.** Therefore, it is possible to explain why NPs have bactericidal activity by pointing to their increased production of ROS and buildup, which frequently causes cell wall break and ultimately culminates in cell demise [40]. Ag-doped TiO_2 NPs shown outstanding antibacterial action against *E. coli,* according to According to Djokic and Burrel [41]**,** Ag ions bind significantly with thiol groups**.** A decrease in the zone of inhibition over time might be brought on by several variables pertaining to the characteristics of the antimicrobial drug, the microbiological population, and the experimental setup [42, 43].

Therefore, it is abundantly evident from the current work that doping NPs can greatly boost antimicrobial action, and that varying the dopant dosage can also greatly boost activity. In light of this, Mn may be regarded as a significant metal dopant that may have antibacterial properties.

It can also be explored as a significant candidate material in subsequent research, which will allow for the investigation of even larger percentages of metal ion doping. Pure and doped ZnS NPs were found to have strong antibacterial action against *Staphylococusaureus, Salmonella typhi, Shigellaflexneri and E. coli* **bacteria**. The pure 15 mol % showed the most activity. Mn-doped ZnS NPs have the ability to successfully stop the growth of *Staphylococusaureus, Salmonella typhi, Shigellaflexneri and E. coli* four bacterial pathogens. The adhesion effectiveness of The increased activity of Mn-doped ZnS is due to the addition of Mn atoms to the bacterial cell walls. It is generally accepted that metal ions bind to cell membranes by interacting with protein thiol groups, deactivating respiratory enzymes and causing reactive oxygen species (ROS) to be produced [43]

Table 2. The antimicrobial activity of ZnS with zone of inhibition

Organism	Zone of inhibition (mm)					Mean value ± SEM	Activity index
	Concentration of ZnS in µg/ml						
	200	400	600	800	1000		
Salmonella typhi	13	14	14	15	17	14.6±1.04	0.7809
Shigellaflexneri	9	10	11	12	14	11.2±0.44	0.7454
Staphylococusaureus	12	13	14	16	18	14.6±2.13	0.7629
E.coli	8	9	9.5	10	11	9.5±0.19	0.5818

Table 3. The antimicrobial activity of ZnS (15mol % Mn doped) with zone of inhibition

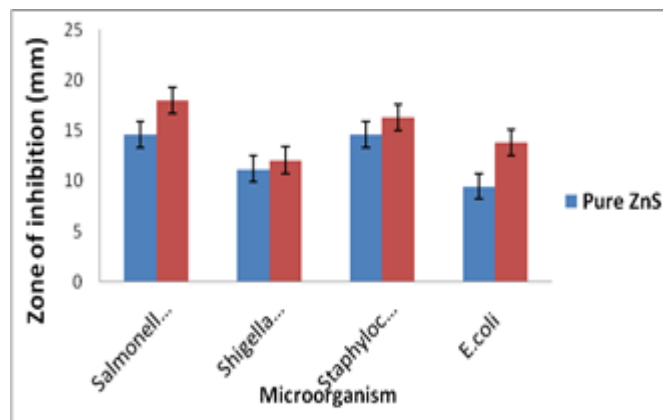| Organism	Zone of inhibition (mm)					Mean value ± SEM	Activity index
	Concentration Mn-doped of ZnS in µg/ml						
	200	400	600	800	1000		
Salmonella typhi	15	17	18	19.2	21.2	18.08±2.02	0.8607
Shigellaflexneri	9	11	12.5	13.7	14.2	12.08±0.04	0.8231
Staphylococusaureus	13	15	16.8	17.9	18.8	16.3±1.12	0.8011
E.coli	11.5	12.7	13.5	15.2	16.3	13.8±0.10	0.7435

Fig. 6. Error bar with standard error for the antimicrobial activity
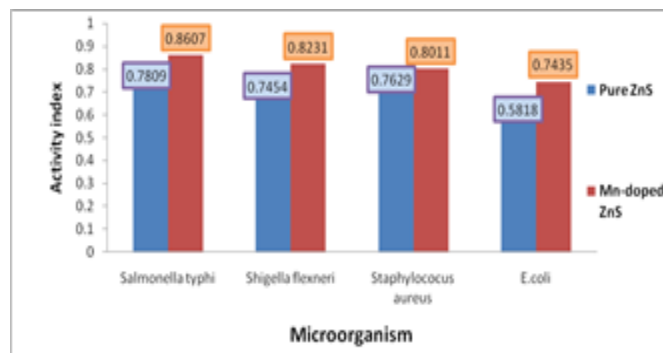

Fig.7. Bar plot for the activity index for samples of pure ZnS and Mn-doped ZnS Nanoparticles

6. Conclusion and Future Scope

By precipitating, manganese-doped ZnS nanoparticles were produced utilizing the sequential reagent addition method (SeqAdd). As a particle regulating agent, methacrylic acid was utilized to control the size and shape of the particles. ZnS nanoparticles were effectively created using an aqueous chemical process having crystallite sizes ranging from 28 to 42 nm on average. It was examined how the structural and optical characteristics were affected by varying calcination temperatures. Both pure and Mn-doped ZnS (15mol %) had pure wurtzite ZnS phase with good crystallinity, according to the XRD data. Both pure and doped ZnS NPs were found to have strong antibacterial action against Salmonella typhi, E. coli, Staphylococusaureus, and Shigellaflexneri. The pure 15 mol % showed the highest activity.

The bacterial pathogens *Shigella flexneri, Salmonella typhi, E. coli,* and *Staphylococcus aureus* could all be efficiently inhibited from growing by Mn-doped ZnS NPs. These promising results show that Mn-doped ZnS NPs have a variety of biological applications. The doped ZnS nanomaterials will be useful in the future for wound healing and hyperthermia treatment. In the commercial market, manganese-based nanoforms can be easily used in conjunction with other substances based on the phases of development, optimization, and appropriate biosafety assessment. Before being used commercially, the other aspects, such as pharmacokinetic studies, immunogenicity, metabolic destiny, and effectiveness, should be thoroughly assessed. The latest article will attract a broader range of the scientific community (both specialized and non-specialized), given that manganese provides a number of benefits in the food, textile, electronics, and water industries in addition to the healthcare industry.

References

[1] L.Chen, Y.Shang, J. Xu, H. Liu, & Y. Hu,"Synthesis of ZnSnanospheres in microemulsion containing cationic gemini surfactant." *J DisperSciTechnol*, Vol.**27**,No.**6**, pp.**839-842, 2006**.

[2] J. Wen, & G. L. Wilkes, "Organic/inorganic hybrid network materials by the sol− gel approach." Chem. Mater, Vol.**8,** No.**8**, pp.**1667-1681, 1996.**

[3] M. Miyake, T. Torimoto, M. Nishizawa, T.Sakata, H. Mori, & H. Yoneyama , "Effects of surface charges and surface states of chemically modified cadmium sulfide nanoparticles immobilized to gold electrode substrate on photoinduced charge transfers." *Langmuir*, Vol.**15**,No.**8**, pp.**2714-2718,1999**.

[4] S. K. Mandal, S. Chaudhuri, & A. K. Pal, "Optical properties of nanocrystallineZnS films prepared by high pressure magnetron sputtering." *Thin Solid Films*, Vol.**350**,No.**1-2**, pp.**209-213, 1999**.

[5] R. Thielsch, T. Böhme, ,& H. Böttcher, "Optical and Structural Properties of Nanocrystalline ZnS-SiO2 Composite Films." *physica status solidi (a)*, Vol.**155**,No.**1**, pp.**157-170 ,1996.**

[6] A.TOMȘA, E. J. Popovici, A.CADIȘ, M. ȘTEFAN, L. Barbu-Tudoran, & S. AȘTILEAN, "Ultrasound-assisted synthesis of highly disperse zinc sulphide powders." *J. Optoelectron. Adv. M.,* Vol.**10**, No.**9**,pp.**2342-2345, 2008.**

[7] B. Bhattacharjee, D. Ganguli, S. Chaudhuri, & A. K. Pal, "ZnS: Mnnanocrystallites in SiO2 matrix: preparation and properties. *Thin solid films*," Vol.**422**,No.**1-2**, pp.**98-103,2002.**

[8] P. Baláž, E.Boldižárová, E.Godočíková& J. Briančin, Mechanochemical route for sulphide nanoparticles preparation. *Mater Lett.* Vol.**57**,No.**9-10**, pp.**1585-1589, 2003.**

[9] J. C. Sanchez-Lopez, & A. Fernandez, "The gas-phase condensation method for the preparation of quantum-sized ZnS nanoparticles." *Thin Solid Films*, Vol.**317**,No.**1-2**, pp.**497-499, 1998.**

[10] J. F. Suyver, S. F. Wuister, J. J. Kelly, & A. Meijerink, "Synthesis and photoluminescence of nanocrystallineZnS: Mn2+". *Nano Lett.,* Vol.**1**, No.**8**, pp.**429-433. 2001.**

[11] W. Sang, Y. Qian, J. Li D. Min, L.Wang, W.Shi, & L. Yinfeng, "Microstructural and optical properties of ZnS: Cu nanocrystals prepared by an ion complex transformation method." *Solid State Commun." ,* Vol.**12**,No.**9-10**, pp.**475-478, 2002.**

[12] Y.Jiang, & Y. J. Zhu, "Microwave-assisted synthesis of nanocrystalline metal sulfides using an ionic liquid." ,Chem.Lett., Vol.**33**, No.**10,** pp.**1390-1391,2004**.

[13] H.J. Bai, Z. M. Zhang, & J. Gong, "Biological synthesis of semiconductor zinc sulfide nanoparticles by immobilized Rhodobactersphaeroides," *Biotechnol.lett,* Vol.**28**, pp.**1135-1139, 2006.**

[14] L. N. Maskaeva, M. A. Lysanova, O. A. Lipina, V. I Voronin, E. A .Kravtsov, A. V., Pozdin, & V. F. Markov, "Structural, optical, and photocatalytic properties of dispersions of CuS doped with Mn2+ and Ni2+". *Kondensirovannyesredyimezhfaznyegranitsy= Condensed Matter and Interphases*, Vol.**26**,No.**2**, pp.**265-279,2024.**

[15] K. Venkatarao, G. Sreedevi, Y. N. Rajeev, B. T. Rao, & S. Cole, "Impact Of Mn2+ Ions On Micro-Structural, Luminescence Properties Of Zns-Mos2 Nanocomposites For Optoelectronics." *Rasayan J. Chem.*, Vol.**15**, No.**1**, pp.**171-182 ,2022**.

[16]M. Mostafa, J. El Nady, S. M. Ebrahim, & A. M. Elshaer, "Synthesis, structural, and optical properties of Mn2+ doped ZnS quantum dots for biosensor application." *Opt. Mater.,* Vol.**112**, pp.**110732, 2021.**

[17] P. Noppakuadrittidej, V. Vailikhit, P.Teesetsopon, S. Choopun, & A. Tubtimtae, "Copper incorporation in Mn2+-doped Sn2S3 nanocrystals and the resultant structural, optical, and electrochemical characteristics."Ceram.Int, , Vol.**44**, No.**12**, pp.**13973-13985, 2018.**

[18] N.Bansal, G. C. Mohanta, & K. Singh, 'Effect of Mn2+ and Cu2+ co-doping on structural and luminescent properties of ZnS nanoparticles." *Ceram. Int.,* Vol.**43**, No.**9**, pp.**7193-7201,2017**.

[19] G. T Rao, R. J. Stella, B. Babu, , K. Ravindranadh, C. V. Reddy, J.Shim, &Ravikumar, R. V. S. S. N, ."Structural, optical and magnetic properties of Mn2+ doped ZnO-CdS composite nanopowder," *MSE: B*, Vol.**201**, pp.**72-78, 2015.**

[20] E. K. Athanassiou, R. N. Grass, & W. J. Stark, "One-step large scale gas phase synthesis of Mn2+ doped ZnS nanoparticles in reducing flames," *Nanotechnol.*, Vol.**21**,No.**21**, pp.**215603, 2010.**

[21] T.Munir, A. Mahmood, A. Ali, N.Abbas, , A. Sohail, Arshia, & Y. Khan," Investigation of antibacterial and anticancer activities of copper, aluminum and nickel doped zinc sulfide nanoparticles," *Scientific Reports*, Vol.**14**,No.**1**, pp.**19304, 2024.**

[22] M.Saroja, M.Venkatachalam, P. Gowthaman, &M.Sathishkumar, "Investigation of Mn doping concentration on the structural, optical, antimicrobial and dye degradation properties of ZnS thin films,", *Mater. Today Proc.* Vol. **43**, pp.**3325-3335, 2021.**

[23] M.Ali, I. M. Ibrahim, E. F. Ahmed, & Q. A. Abbas,"Structural and characteristics of manganese doped zinc sulfide nanoparticles and its antibacterial effect against gram-positive and gram-negative bacteria,"*Biophys,* Vol.**6**,No.**1**,**2016.**

[24] M. Kawsar, M. S. Hossain, N. M. Bahadur, & S. Ahmed, " Synthesis of nano-crystallite hydroxyapatites in different media and a comparative study for estimation of crystallite size using Scherrer method, Halder-Wagner method size-strain plot, and Williamson-Hall model," *Heliyon*, Vol.**10**,No.**3**.

[25] A. K. Zak, W. A.,Majid, M. E. Abrishami, & R. Yousefi, "X-ray analysis of ZnO nanoparticles by Williamson–Hall and size–strain plot methods," *Solid State Sci.*, Vol.**13**,No.**1**, pp.**251-256, 2011**.

[26] R. Ghamarpoor, A. Fallah, & M. Jamshidi, "A review of synthesis methods, modifications, and mechanisms of ZnO/TiO2-based photocatalysts for photodegradation of contaminants," *ACS omega*, Vol.**9**,No.**24**, pp.**25457-25492,2024.**

[27] R.Das, & S.Sarkar,"Determination of intrinsic strain in poly (vinylpyrrolidone)-capped silver nano-hexapod using X-ray diffraction technique,"*Curr. Sci*,pp.**775-778, 2015**.

[28] P. S. Sundaram, T. Sangeetha, S. Rajakarthihan, R. Vijayalaksmi, A. Elangovan, & G. Arivazhagan, "XRD structural studies on cobalt doped zinc oxide nanoparticles synthesized by coprecipitation method: Williamson-Hall and size-strain plot approaches," *Physica B: Condens. Matter*, Vol. **595**, No.**412342,2020**.

[29] S.Mustapha, M. M. Ndamitso, A. S. Abdulkareem, J. O.Tijani, D. T. Shuaib, A. K.Mohammed, & A. Sumaila, "Comparative study of crystallite size using Williamson-Hall and Debye-Scherrer plots for ZnO nanoparticles," AFSN, Vol.**10**,No.**4**, pp.**045013, 2019.**

[30] D.Nath, F. Singh, & R. Das, "X-ray diffraction analysis by Williamson-Hall, Halder-Wagner and size-strain plot methods of CdSe nanoparticles-a comparative study." *Mater. Chem. Phys,* Vol.**239**, pp.**122021.2020**.

[31] R. Kripal, A. K.Gupta, S. K. Mishra, R. K. Srivastava, A. C. Pandey, & S. G. Prakash, "Photoluminescence and photoconductivity of ZnS: Mn2+ nanoparticles synthesized via co-precipitation method," *SpectrochimicaActa Part A:*, *SpectrochimActa A MolBiomol Spectrosc*,Vol.**76**,No.**5**, pp.**523-530, 2010.**

[32] P. Nwaokafor, K. B. Okeoma, O. K. Echendu, A. C. Ohajianya, & K. O. Egbo, "X-ray diffraction analysis of a class of AlMgCu alloy using williamson–hall and scherrer methods," *Metallogr. Microstruct.Anal*.Vol. **10**, pp.**727-735, 2021.**

[33] N. Wang, Y.Yang, & G. Yang, "Great blue-shift of luminescence of ZnO nanoparticle array constructed from ZnO quantum dots." *NanoscaleRes.Lett*, Vol.**6**, pp.**1-6, 2011.**

[34] V. H. T. Thi, & B. K. Lee,"Effective photocatalytic degradation of paracetamol using La-doped ZnOphotocatalyst under visible light irradiation." ,*Mater. Res.Bull,* Vol.**96**, pp.**171-182. 2017.**

[35] R. Ponnusamy, S. C. Selvaraj, M. Ramachandran, P. Murugan, P. M. G. Nambissan, & D. Sivasubramanian, "Diverse spectroscopic studies and first-principles investigations of the zinc vacancy mediated ferromagnetism in Mn-doped ZnO nanoparticles," *Cryst Growth Des*,Vol.**16**,No.**7**, pp.**3656-3668. 2016.**

[36] D.Li, J.Hu, F.Fan, S.Bai, , R. Luo, A.Chen& C. C Liu, "Quantum-sized ZnO nanoparticles synthesized in aqueous medium for toxic gases detection." *J. Alloys Compd,* Vol.**5**,No.**39**, pp.**205-209, 2012.**

[37] K. SowriBabu, A. Ramachandra Reddy, C. Sujatha, K. Venugopal Reddy, & A. N. Mallika, "Synthesis and optical characterization of porous ZnO." *J. Adv. Ceram,* Vol. **2**, pp.**260-265, 2013**.

[38] K. V. S. Rao, B. Lavédrine, & P. Boule,"Influence of metallic species on TiO2 for the photocatalytic degradation of dyes and dye intermediates," *J. Photochem. Photobiol, B A: Chemistry*, Vol.**154**,No.**2-3**, pp.**189-193,2003.**

[39] K. R. Raghupathi, R. T. Koodali, & A. C. Manna,"Size-dependent bacterial growth inhibition and mechanism of antibacterial activity of zinc oxide nanoparticles." *Langmuir*, Vol.**27**,No.**7**, pp.**4020-4028,201.**

[40] J.Thiel , L. Pakstis, S. Buzby, M. Raffi, , C. Ni, D. E. Pochan, & S. I. Shah, "Antibacterial properties of silver-doped titania." *Small*, Vol.**3**, No.**5**, pp.**799-803,2007.**

[41] S. S. Djokić, & R. E. Burrell, "Behavior of silver in physiological solutions.", *J. Electrochem. Soc,* Vol.**145**, No.**5**, pp.**1426, 1998**.

[42] U. Srivastava, A. Singh, M. Ahmed, U. Iqbal, & P. Saini, "Functional and physicochemical characterization of a novel pearl millet—Soy milk-based synbiotic beverage." *Food Safety and Health,***2024**.

[43] Y. Matsumura,K.Yoshikata, S. I. Kunisaki, & T. Tsuchido, "Mode of bactericidal action of silver zeolite and its comparison with that of silver nitrate." *AEM*, Vol.**69**, No.**7**, pp.**4278-4281, 2003**.

AUTHORS PROFILE

Mr. JanmejayYadav, born on July 15, 1994, developed a strong interest in science, mathematics, and literature during his high school years. He completed his graduation from V.B.S.P.U., Jaunpur, He did M.Sc. in Physics from Nehru Gram Bharati, Prayagraj.Currently, he is pursuing Ph. D. from NGB DU, Prayagraj on the topic 'Characterization of Mn^{2+} doped nanocomposite of metal oxide and sulfide nanocrystals' He has authored several research papers in reputable international journals on her subject.

Dr. Vikram Singh is working as Assistant Professor at physics Department of Nehru Gram Bharati Deemed to be University, Allahabad. He works in Quantum Optics, Non Linear Optics, EPR and Nano Composites. His research papers have been published in several reputable international journals which have been cited by several other workers.

Prof. Ram Kripal received his Ph.D. degree in Physics from Allahabad University, India in the area of condensed matter physics. His current research interests are in both theoretical and experimental EPR (Electron Paramagnetic Resonance, also called ESR, Electron Spin Resonance). His research laboratory includes Varian X-band(9.5 GHz) CW(continuous wave) EPR spectrometer operational in the 77-1000K temperature range and Unicam 5636 UV/Visible spectrophotometer operating in the wavelength range 195-1100 nm. He collaborates actively with researchers at NPL (National Physical Laboratory), New Delhi, India and with Prof. C. Rudowicz, Faculty of Chemistry, A. Mikowicz. University,

Poznan, Poland. In addition to polycrystalline and single crystal CW EPR he does optical absorption in the wavelength range mentioned above. He is also engaged in EPR research of nano-materials. 20 Ph.D. students have received their degrees under his supervision. He has acted as an external examiner to several Ph.D. and M. Phil. theses examinations outside Allahabad University. He serves as a referee to important journals in physical sciences which publish EPR research (J. Phys. Chem. Solids, Solid State Commun., J. Magn. Magn Material, Spectrochim. Acta, J. Mat. Sci., J. Alloys and Comp., Chem. Phys., Chem. Phys. Lett., Phys. Scripta, J. Magn. Reson., Indian J. Phys.). He has published several articles in EPR and has written a book on Practical Physics, Introduction to Electromagnetic Theory. His research has been continuously supported by UGC (University Grants Commission), CSIR (Council of Scientific and Industrial Research), DST (Department of Science and Technology) and CST (Council of Science and Technology), India

Dr Rajesh Kumar Yadav is Assistant professor at Department of Physics, CMP Degree College, University of Allahabad, Prayagraj, India.
He earned BSc, MSc and PhD from VBS University Jaunpur, India. He worked as assistant professor in UG, Department of Physics Sardar Patel Mahavidyalay, Larpur, Ambedkar Nagar (Dr RML Avadh University, Faizabad) from July 2005 to Dec. 2013 and HCPG College Mahatma Gandhi Vidyapeeth Varanasi from Dec. 2013 to Nov. 2017. He is a member of "Vigyan Parishad" academy of Prayagraj. He has published research papers in reputed international journals like Spectrochimacta Part A, Indian journal of Physics, IJRES, IJCRT on Molecular Spectroscopy and nanoparticles Physics.

Dr. Urvashi Srivastava received her Ph. D degree from Centre of Food Technology, University of Allahabad, India in Nutritional Sciences, Her research work was undertaken to explore the effect of fermentation (natural and probiotic fermentation) on the physicochemical properties and functional components of selected millets along with development of multifunctional value added non-dairy probiotic products. Currently working as Assistant Professor of Home Science at Om Mahavidyalay PG College, Sikandra (affiliated to Allahabad State University). She is also taking classes of Nutritonal sciences, Food processing and other vocational courses of UG and PG classes as per New Education Policy (NEP) norms. She also worked as an Analyst (testing of food and water samples) at NABL accredited Food Analysis & Research Laboratory, Centre of Food Technology, Institute of Professional Studies, University of Allahabad. Her research papers have been published in several reputed international journals of Elsevier, Springer, Wiley etc. which have been cited by several other workers.